A&A 462, 637–644 (2007)
DOI: 10.1051/0004-6361:20065264

Astronomy & Astrophysics

A 1.2 mm MAMBO survey of post-AGB stars

C. S. Buemi[1], G. Umana[1], C. Trigilio[1], and P. Leto[2]

[1] INAF, Osservatorio Astrofisico di Catania, via S. Sofia 78, 95123 Catania, Italy
e-mail: cbuemi@oact.inaf.it
[2] INAF, Istituto di Radioastronomia, Sezione di Noto, CP 161, 96017 Noto (SR), Italy

Received 24 March 2006 / Accepted 26 September 2006

ABSTRACT

Aims. We performed a millimetric survey of a sample of 24 post-AGB stars aimed at searching for emission from circumstellar matter, in order to investigate the physical properties of the outer parts of the envelopes.
Methods. The observations were conducted using the 37-channel Max-Planck Millimeter Bolometer array at the 30-meter IRAM telescope. The continuum emission toward the detected sources was used to quantify the mass of the emitting dust. We combined our observations with data available in the literature to construct the spectral energy distribution (SED) of the sources. When the observational data covered a spectral range wide enough, some properties of circumstellar envelopes were derived by comparison with spectra computed using a radiative transfer code.
Results. Of the 24 objects in our sample, we detected millimetric continuum emission toward 11 sources. Two other sources were detected at a flux level close to 3σ. The derived circumstellar dust masses range between 0.4 and 24×10^{-4} $M_{\odot}$, but these results are affected by the uncertainty about the source distances. The parameters derived from the SED fits are consistent with the values characteristic of this kind of object. As confirmed from the flux density extrapolated in the first light channels of the Atacama Large Millimetric Array, these sources could be good targets for future high-resolution mapping with the ALMA facility.

Key words. stars: AGB and post-AGB – circumstellar matter – planetary nebulae: general– radio continuum: stars

1. Introduction

Stars on the red giant branch undergo a process of copious mass loss leading to the formation of a circumstellar envelope (CSE). These envelopes, quilted up by the ejected material, contain atomic and molecular gas and are characteristic of the post asymptotic giant branch (AGB) evolutionary phase, which results in the formation of a planetary nebula (PN). Because of the huge amount of processed material returned to the ISM, this evolutionary phase is very important for the chemical evolution of the Galaxy; and yet the short transition phase between the end of the AGB and the formation of a new PN is still poorly understood. In particular, it is quite challenging to understand how the almost symmetric CSE observed around AGB stars transform themselves in to the highly structured morphologies observed in high-dynamical range optical images of PNs.

The importance of studying objects on this way to becoming PNs resides in how the unknown physical mechanisms that shape the PNs in their CSE are already at work, as HST images of multi-polar outflows in post-AGB stars appear to indicate (Sahai 2001). Despite numerous efforts to identify the shaping agent/s in PNs (Sahai & Trauger 1998; Garcia-Segura et al. 2005), there is no observational evidence to support one mechanism over the others (Balick & Franck 1002).

Dust is ubiquitous in post-AGB and PN sources, and quite often it is in the form of disks and tori. Some models evoke these structures, whose origin is under debate, however, as an important ingredient in the mechanism that produces the collimated outflows observed in the CSE (Frank et al. 1997; Huggins et al. 2004). In this context, very important information can be provided by studying the physical properties of CSE and, in particular, the presence and spatial distribution of the circumstellar dust, as this may help in finding clues to the nature of the shaping agent.

Detailed studies of the spectral energy distribution (SED) of a small sample of optically bright post-AGB candidate stars have shown that these objects can be divided into two groups, depending on the shape of the IR excess (Trams et al. 1991; van der Veen et al. 1994): sources with a broad IR excess extending from the near infrared until the far-IR have both hot and cool dust in their circumstellar shells, and sources with a far-IR excess only show the presence of cool dust. The double peaks in the SEDs appear to be characteristic of objects in transitions, but the presence of only cool dust seems to point to objects that are more evolved towards PNs. Thermal emission from dusty envelopes may extend up to millimiter wavelengths, depending on the temperature of the dust. In particular, millimetric observations are essential for determining the SEDs of the sources better and thus putting more stringent constraints on the model of their circumstellar envelopes. Moreover, millimetric observations allows us to attest to the presence of multiple dusty shells that are related to different mass-loss episodes by the stars.

In this paper we present the results of a 1.2 mm survey aimed at detecting the millimetric emission from a sample of post-AGB stars for a robust modeling of their circumstellar envelopes. This appears as a first necessary step in preparing for the use of the new interferometers (i.e. ALMA and CARMA) that, in the very near future, will be able to resolve, in unprecedented spatial resolution, the circumstellar geometry and thus a full understanding of the shaping mechanisms.

Table 1. Properties of stars in our sample, where the *IRAS* fluxes come directly from the Point Source Catalog (PSC).

Sources with optical counterpart						
IRAS name	RA(J2000)	Dec(J2000)	F_{12} [Jy]	F_{25} [Jy]	F_{60} [Jy]	F_{100} [Jy]
00210+6221	00 23 51.2	+62:38:16	48.5	51.9	12.5	<23.2
01174+6110	01:20:44.9	+61:26:18	4.1	16.9	33.9	4.1
04296+3429	04:32:56.6	+34:36:11	12.7	45.9	15.4	<9.2
05089+0459	05:11:36.1	+05:03:26	7.4	21.9	11.9	3.8
06530–0213	06:55:32.1	−02:17:30	6.1	27.4	15.1	4.1
07134+1005	07:16:10.2	+09:59:48	24.5	116.7	50.1	18.7
07331+0021	07:35:41.1	+00:14:58	15.3	68.1	18.5	3.7
17436+5003	17:44:55.4	+50:02:39	6.1	184.0	152.0	48.7
19114+0002	19:13:58.6	+00:07:31	31.3	648.3	515.9	168.1
20000+3239	20:01:59.4	+32:47:32	15.0	71.0	30.0	<43.1
20028+3910	20:04:35.0	+39:18:38	41.8	210.8	143.1	46.5
22223+4327	22:24:30.6	+43:43:03	2.1	37.1	22.4	9.5
22272+5435	22:29:10.3	+54:51:06	73.9	302.4	96.6	41.0
22574+6609	22:59:18.4	+66:25:48	9.0	29.5	10.7	2.5
23304+6147	23:32:45.0	+62:03:49	11.4	59.1	26.6	7.2
Sources without optical counterpart						
07430+1115	07:45:49.8	+11:08:25	7.7	22.9	10.7	2.5
18454+0001	18:48:01.5	+00:04:47	10.8	14.5	13.6	<384
18514+0019	18:53:57.9	+00:23:24	4.9	23.4	17.3	<152
18576+0341	19:00:11.2	+03:45:46	58.5	425.0	274.7	<1660
19024+0044	19:05:01.5	+00:48:48	2.9	48.8	42.5	15.7
19075+0432	19:10:00.0	+04:37:06	5.2	28.1	31.8	14.4
19454+2920	19:47:24.3	+29:28:12	17.3	89.6	54.4	14.7
20144+4656	20:15:58.3	+47:05:39	1.2	17.0	20.0	<85
21537+6435	21:55:04.6	+64:49:54	6.9	26.1	13.3	<6.1

2. Observations

In trying to determine a possible millimetric emission due to thermal dust emission from the circumstellar envelope, we observed a sample of Post-AGB stars with the 30 m IRAM telescope.

Since the dusty envelopes show a clear signature of the stars in the far-IR spectrum, the IRAS colour-colour diagram has been successfully used by several authors in systematic searches for post-AGB objects by looking for sources in-between the locus of the planetary nebulae and late-type AGB stars. Garcia-Lario et al. (1997) compiled a list of stellar objects, characterised by strong F-IR excess, which occupy the same region of the IRAS colour diagram as AGB stars and PNs. The sample contains 126 post-AGB. Among those, a large fraction (70%) represent post-AGBs in a very early stage, still heavily obscured in the optical.

Another method of looking for transition objects is concentrated on optically bright objects with an IR excess due to circumstellar dust (Pottash & Parthasarathy 1988; Trams et al. 1991; Oudmaijer et al. 1992). These resulted in the detection of objects scattered in the IRAS colour-colour diagram, as they show different amounts of IR excesses and different IR-colours.

Oudmaijer et al. (1992) and Oudmaijer (1996) looked for transition objects with an optical counterpart by performing a cross-correlation of the SAO optical catalogue with the IRAS point-source catalogue, selecting supergiants with a spectral type between B and G and with an IR excess due to circumstellar dust.

To select a sample of possible targets, we used the most complete compilations of objects with no optical counterpart, from Garcia-Lario et al. (1997) and of objects with optical counterpart from Oudmaijer et al. (1992) and Oudmaijer (1996), selecting the stars identified as post-AGB, which are associated with highly evolved post-AGB stars with low-mass progenitors. We further included in the sub-sample of stars with optical counterpart 11 stars, originally not classified by Oudmjier et al. (1992) as post-AGB, for which there compelling observational evidence that they are in the post-AGB evolutionary stage (van der Veen et al. 1994; van Wincker 1997).

A small sample of post-AGB stars has been observed in the millimetric band with the JCMT (van der Veen et al. 1994), and the detection rate appeared to be well-correlated with the F_{60} IRAS flux, in the sense that all the stars with $F_{60} \geq 10$ Jy have been detected. If the extra infrared excess has the shape of a cold black body, as expected from a more distant dust shell, an F_{60} of $\sim$10 Jy would imply a 1.3 mm flux higher than 36 mJy and thus easily detectable with the new Bolometer. In order to maximise the probability of having a detectable flux at 1.2 mm, we thus selected only those sources with $F_{60} \geq 10$ Jy from our original sample. This reduces our sample to 34 targets.

In this section we report on the results relative to a subsample of 24 objects, which are given in Table 1.

2.1. The 30 m IRAM observations and results

The 37-channel Max-Planck Millimeter Bolometer ("MAMBO"; Kreysa et al. 1998) array at the 30-meter IRAM telescope on Pico Veleta (Spain) was used to perform this survey. The observations were made between 21 January and 7 February 2002, using the standard ON-OFF technique, performed by chopping the secondary mirror of the telescope by about 50″ in azimuth at a rate of 1 Hz. The FWHP of our beam was 10.″5 at 1.2 mm.

For each source, the observations were typically obtained in blocks of 4 or 5 scans lasting 4 min each. Frequent skydip observations were used to determine atmospheric extinction as a function of elevation and time. The data were analysed with the MOPSI software (Zylka 1998). The flux calibration was performed by observing either Mars or Uranus to determine the flux conversion factor. For each channel the sky noise was subtracted

Table 2. Measured millimeter fluxes.

IRAS name	Date	Time [s]	Flux [mJy]	Weather†
Sources with optical counterpart				
00210+6221	21 Jan. 02	1200	... ± 2.4	B
01174+6110	21 Jan. 02	1200	22.9 ± 1.7	B
04296+3429	14 Feb. 02	1200	4.4 ± 1.3	A
05089+0459	05 Feb. 02	1440	... ± 1.0	A
06530−0213	14 Feb. 02	1200	4.8 ± 1.5	A
07134+1005	07 Feb. 02	1200	14.0 ± 1.5	A
07331+0021	07 Feb. 02	1200	... ± 1.9	B
17436+5003	05 Feb. 02	1080	15.2 ± 1.1	A
19114+0002	04 Feb. 02	480	68.2 ± 3.4	B
20000+3239	21 Jan. 02	1200	11.4 ± 1.7	B
20028+3910	21 Jan. 02	1200	11.9 ± 1.5	A
22223+4327	04 Feb. 02	1200	... ± 1.5	A
22272+5435	04 Feb. 02	1200	35.3 ± 1.7	A
20144+4656	21 Jan. 02	1200	... ± 1.8	B
23304+6147	21 Jan. 02	1200	... ± 1.8	B
Sources without optical counterpart				
07430+1115	07 Feb. 02	1200	... ± 1.3	A
18454+0001	22 Jan. 02	1200	... ± 1.4	A
18514+0019	21 Jan. 02	1200	8.2 ± 1.3	A
18576+0341	03 Feb. 02	840	≥45.4 ± 2.2	B
19024+0044	22 Jan. 02	1200	... ± 1.3	A
19075+0432	04 Feb. 02	1200	6.2 ± 1.2	A
19454+2920	03 Feb. 02	1200	... ± 4.3	C
20144+4656	05 Feb. 02	1200	... ± 2.7	C
21537+6435	04 Feb. 02	1200	6.3 ± 1.6	A

† Wheather condition: A: good, B: poor, C: bad.

by computing the weight mean of the signals from the surrounding six channels.

In Table 2, the resulting 1.2 mm flux densities measured for the detected objects are reported. Out of the 24 observed sources, we carried out 11 detections over the threshold of 4σ and two uncertain detections at 3σ. Four of the detected and one of the undetected sources overlap the sample observed by Walmsley et al. (1991), using the 30 m IRAM telescope at the wavelength of 1.3 mm, but with a different bolometer. The measured flux densities accord well with the exception of IRAS 22272+5435, which shows a significatively higher flux level.

The sample includes IRAS 01174+6110 and IRAS 18576+0341, which were first classified as post-AGB stars on the basis of their IRAS colours, but probably had a different nature. IRAS 01174+6110 is very likely an HII region (Kelly et al. 2005), while IRAS 18576+0341 was recently recognised as a new LBV (Pasquali & Comeron 2002; Clark et al. 2003; Umana et al. 2005). For these two objects we just report the measured flux density.

In particular, IRAS 18576+0341 will be the object of a more detailed future analysis assembled with high-resolution radio results. Umana et al. (2005) points out that the source's right ascension is shifted about 4″ with respect to values previously reported in the literature (Garcia-Lario 1997). Since the first contour level in the 22 GHz map defines a source size close to 10″, it is reasonable to consider the measured 1.2 mm flux as a lower limit.

Some of the detected objects in our sample have been detected in ^{13}CO and/or ^{12}CO transition $J = 2{-}1$ at $\lambda = 1.3$ mm, which is within the band of our observations (Hrivnak et al. 2005; Bujarrabal et al. 1992; Bujarrabal et al. 2001). We verified that the contribution of this emission, spread in our bandwidth of about 80 GHz, is lower than the errors associated to the measures for all the detected sources except IRAS 19114+0002 and IRAS 22272+5435. In particular, on the basis of the observations by Bujarrabal et al. (1992), we derived an emission in the MAMBO band for IRAS 19114+0002 of 15 mJy from ^{12}CO and of 1.6 mJy from ^{13}CO; for IRAS 22272+5435, the contribution of ^{12}CO emission is about 7 mJy (Hrivnak et al. 2005). In the following calculations, we thus subtracted these contributions from the observed fluxes.

2.2. Spectral energy distributions

In order to build up the SED of the detected sources, updated with our millimetric data, and to investigate its corrected low-frequency shape, we combined our MAMBO observations with the infrared (2MASS + IRAS + MSX) and optical data available in the literature. The data are corrected for the interstellar extinction, with the exception of IRAS 19075+0432, due to the lack of information about the extinction toward the source. Moreover, we excluded IRAS 01174+6110 from this analysis because of the uncertainty on its nature.

For those objects for which the observations cover a wide enough spectral range, the resulting SEDs (Fig. 1) show the typical double-peaked shape, with the two peaks corresponding respectively to the optical emission from the photosphere of the central star and to the thermal emission from the circumstellar dust.

3. Analysis

3.1. Dust masses

From a theoretical point of view, the mass of the circumstellar dust surrounding the central object can be derived from the observed continuum millimetric flux. Assuming that the flux density measured at this frequency is to be ascribed to the thermal emission from optically thin and isothermal dust, the dust mass (M_d) and the flux density are directly proportional (Hildebrand 1983):

$$M_\mathrm{d} = \frac{F(\nu)d^2}{B_\nu(T_\mathrm{d})\chi_\nu}$$

where $B_\nu(T_\mathrm{d})$ is the Planck function for dust temperature T_d, d the distance to the source, and χ_ν the dust opacity at the observing frequency. We can thus estimate the dust mass by using the Rayleigh-Jeans approximation:

$$M_\mathrm{d} = \frac{F(\nu)\lambda^2 d^2}{2kT_\mathrm{d}\chi_\nu}. \quad (1)$$

The value of χ_ν is the major uncertainty that affects the conversion of the millimetric flux density in dust mass. Following Hildebrand's approach, we can extrapolate the dust opacity χ_ν at 1.2 mm from its value at 250 μm, i.e. $\chi_{250\,\mu\mathrm{m}} = 10\ \mathrm{cm^2\,g^{-1}}$, assuming the power-law dependence $\chi_\nu \propto \nu^p$, where p is the emissivity index that strongly depends on the mineralogical composition of the grain and on their physical shape.

Under the hypothesis of optically thin emission, the emissivity index p may be derived from the spectral index in the millimetric and submillimetric spectral ranges, where the dust emits as a blackbody modified by the frequency-dependent dust opacity, that is, $F_\nu \propto \chi_\nu B_\nu(T_\mathrm{d})$.

We thus proceeded iteratively by fitting a modified blackbody to the infrared and millimetric data to estimate the dust

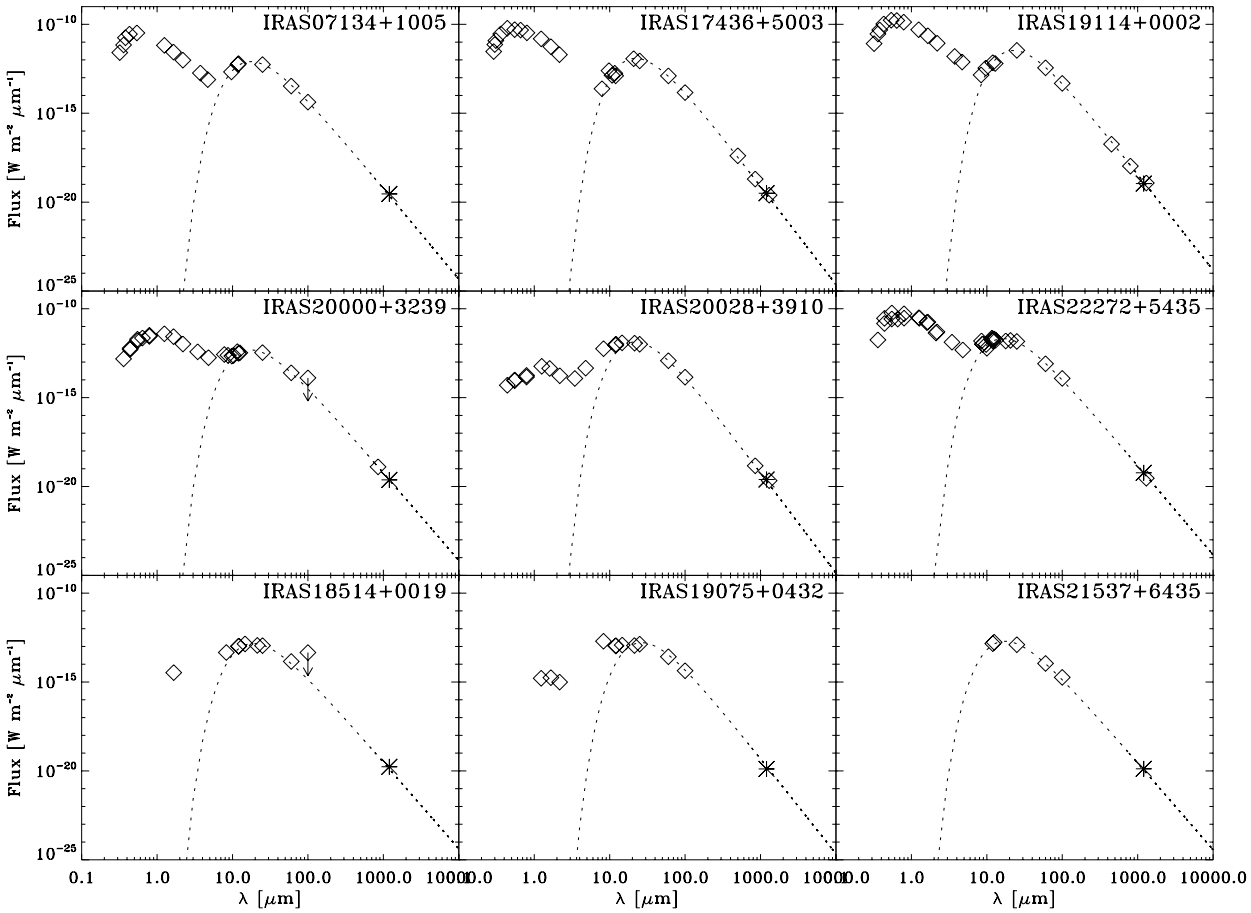

Fig. 1. Spectral energy distributions of the emission towards the detected sources. The asterisks indicate measures from this work. The dashed lines show the modified blackbody fits to the long-wavelength data, as discussed in the text (Sect. 3.1).

temperature, while the emissivity index was derived from a linear fit in the $\log \nu - \log \frac{F_\nu}{B(T_d)}$ to the integrated flux density from 100 μm to 1.2 mm. In the case of IRAS 19075+0432, we note that the MSX data at 8.28 μm suggest the presence of both warm and cold circumstellar dust.

For sources with only an upper limit on IRAS 100 μm flux, the same analysis was performed using the IRAS 60 μm flux to constrain the minimum value for p. In Fig. 1 the resulting curves are overplotted to the observed SEDs. In Table 3 the best-fit parameters are listed together with the derived dust opacities and masses calculated from Eq. (1) for $\lambda = 1.2$ mm.

3.2. SED modeling with DUSTY code

For six of the detected post-AGB stars, the observations scan a wide spectral range between optical bands and radio regions. All the available information on the sources, including the results from SED fits with envelope models, were collected from the literature, in order to verify the compatibility of the previously determined parameters with our 1.2 mm fluxes.

The observed SEDs are plotted in Fig. 3, along with the best-fit SEDs from the radiative transfer code DUSTY (Ivezič et al. 1999). This code allowed us to calculate the radiative transfer through a spherically symmetric dust shell and to determine the SED on the basis of specified properties of the radiation source, dust composition, and dust shell properties. In particular, DUSTY allows the use of six different types of dust grains that are assumed to be distributed in a spherical shell. For all the sources, we assumed Planckian SED for the central star and the modified MRN (Mathis et al. 1977) power law for the grain-size distribution $n(a) \propto a^{-q}$, where a is the grain-size and q is fixed to 3.5, as is common if not otherwise specified in the text. For more details about the other options, we refer the reader to the description in the user manual. When available, we calculated the SED by assuming the stellar and dust parameters taken from previous references in the literature; otherwise, the best-fit model parameters are sought iteratively by fitting the shape of the observed SED. With the aim of adding more observational constraints, we

Table 3. Derived values for the emissivity index, dust mass, absorption coefficient, and envelope dust mass.

IRAS name	T_d [K]	p	$\chi_{1.3}$ [cm^2 g^{-1}]	M_d [$M_\odot$]	d [kpc]
Source with optical counterpart					
07134+1005	135	1.11	1.75	8.5 (–4)	2.4
17436+5003	100	1.55	0.88	6.2 (–4)	1.2
19114+0002	100	1.41	1.09	4.3 (–2)	6.0
20000+3239	140	0.94–1.55	0.88–2.1	0.9–2.3 (–4)	1.0†
20028+3910	100	1.65	0.75	2.4 (–3)	2.9
22272+5435	145	1.03	1.98	6.2 (–4)	1.6
Source without optical counterpart					
18514+0019	130	0.89–2.18	0.32–2.5	0.6–4.8 (–4)	1.0†
19075+0432	85	1.37	1.2	1.5 (–4)	1.0†
21537+6435	140	0.87–0.97	2.18–2.55	4.3–5.1 (–5)	1.0†

† Assumed distance.

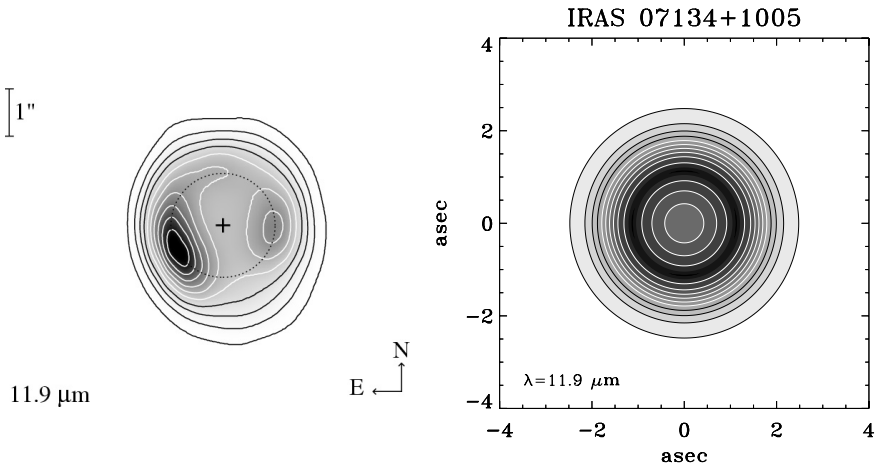

Fig. 2. *Left*: image of IRAS 07134+1005 observed at 11.9 μm by Hony et al. (2003). *Right*: the map simulated at 11.9 μm using the DUSTY code, assuming the parameters reported in Table 4. The map has been convolved with a circular beam with an *HPBW* of 0.″83. In both the maps, the contours indicate the 5–95% intensity levels in steps of 10%.

compared the infrared maps of the sources available in the literature with the simulated maps obtained from the code at the same observational frequencies. All the simulated maps were convolved with the beam of the instrument to obtain the map used for comparison. An example of such a comparison is shown in Fig. 2 in the case of IRAS 07134+1005. In particular we refer to Hony et al. (2003) for IRAS 07134+1005, Gledhill et al. (2003) for IRAS 17436+5003, Jura & Werner (1999) for IRAS 19114+0002, Ueta et al. (2001) for IRAS 22272+5435, and to the 2MASS Atlas image provided from Infrared Science Archive (`bungo.ipac.caltech.edu/applications/2MASS/IM/interactive.html`) for IRAS 20000+3239 and IRAS 20028+3910. We thus rejected all those solutions that involve shell sizes that do not match the observational constraints according to the rms noise level of the measures.

The remaining four sources of our sample, as detected in the survey, were not fitted because of the lack of either data or knowledge of stellar parameters, that make to involve too many degrees of freedom in the fit.

A summary of the adopted input parameters used to produce the model fits in Fig. 3 is given in Table 4. In addition, we report the derived stellar and dust-shell parameters besides the physical quantities used in scaling the dusty outputs in accordance with the dusty manual (Ivezič et al. 1999). In all calculations we assumed a density for the grain material of 3 g/cm^3 and a gas/dust ratio of 220.

The fit's parameter, which is mainly constrained from the millimetric and submillimetric measures, is the shell outer radius, as these observations probe the cool outer parts of the CSE. However, the value derived from the SED fit and reported in Table 4 has to be meant as an estimate of the distance from the star where the wind density is close to the ambient density. Thus, the modeled envelope could result in being more extended than the observed one, if its outer parts come to have a surface brightness lower or equal to the rms noise level. In particular, it is not surprising that the radii derived for the CSE outer edge result in being much greater than those derived from the near or mid infrared observations, since at those frequencies most of the flux comes from the hotter inner regions of the envelope.

On the basis of the mass-loss rate and shell size derived from the SED fit, we calculated the total envelope mass, assuming a constant wind expansion velocity that was taken from references in the literature. The dust envelope masses derived for a gas/dust ratio of 220 are also reported in Table 4. Such values are consistent with those reported in Table 3 within a factor of 2. We can thus determine that there is good agreement between the two dust mass estimates, expecially given the rough approximations made in the assumption of constant mass-loss rate and in the choice of the gas/dust ratio, which could differ significantly from the assumed value as a function of the C/O ratio.

4. Results and discussion

This section discusses the fit of the model to the observed flux distribution. For each sources, the results of the modeling are compared with the calculations and measures obtained from other authors.

IRAS 07134+1005. This object is known to have strong features near 21 and 30 μm, whose carrier species have not yet been firmly identified (Kwok et al. 1989). It is an F5 supergiant with C/O $\approx$ 1 (Van Winckler & Reyniers 2000). Despite the very simplified dust composition used in our model calculations, the parameters derived from our fit accord well with the ones calculated from Meixner et al. (2004) and Hony et al. (2003), using different dust radiative transfer programs, with the exception of the mass loss rate that is higher by a factor of 3 than the one calculated from Hony et al. (2003). On the other hand, our derived value for $\dot{M}$ agrees with the values obtained from the SED model performed by Hrivnak et al. (2000) and from Jura et al. (2000) on the basis of their mid-IR images of the source.

IRAS 17436+5003 is a F3 Ib supergiant with an oxygen-rich chemistry (Justtanont et al. 1992). Its SED has been modeled by several authors by adopting different choices mainly in the selection of grain parameters. While Hoogzaad et al. (2002) and Meixner et al. (2002) adopt the usual grain-size distribution $n \propto a^{-3.5}$ with a minimum size of 0.18 μm and 0.2 μm, respectively, Gledhill & Yates (2003) opt for very small grains, using a steep size distribution $n \propto a^{-6}$ and minimum grain-size of 0.01 μm, which account better for both the SED shape within the whole frequency range and the observed high degrees of near-IR linear polarization, as pointed out by the authors. In our calculation we followed the latter way. As a consequence, the dust mass reported in Table 3 could be underestimated because the assumed dust opacity is derived from an approximated grain model with an average grain size of 0.1 μm

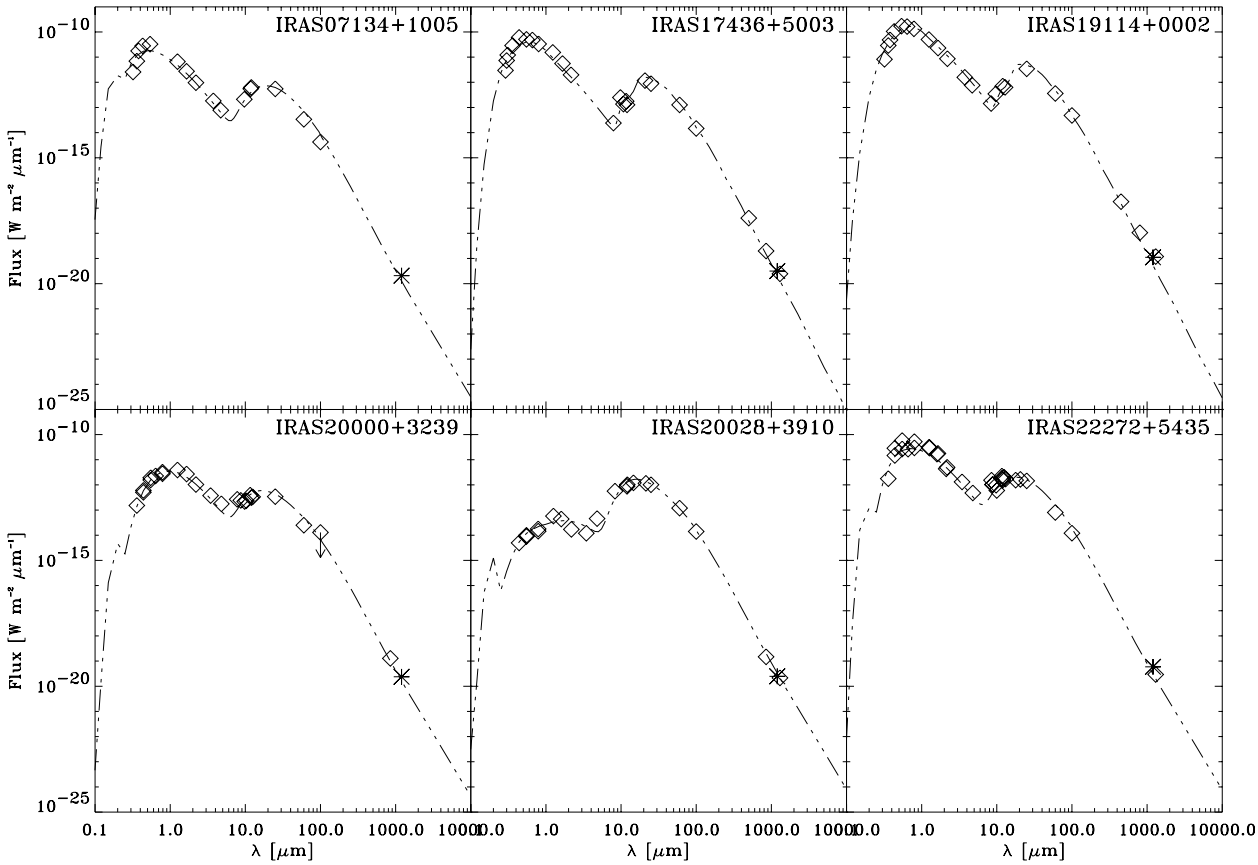

Fig. 3. Spectral energy distributions of the emission towards six stars in the sample. The asterisks indicate measures from this work. The dashed lines show the SEDs computed using the DUSTY code.

Table 4. Input and derived stellar and dust parameters resulting from the fit to the SED.

Property	IRAS	07134+1005	17436+5003	19114+0002	20000+3239	20028+3910	22272+5435
T_*[K]		7250	7500	5660	5000	7000	5300
Chem.		C	O	O	C	C?	C
T_d[K]		150	120	110	170	180	160
L [$L_\odot$]		6000	3440	300000	630	6600	6700
A_V		0.5	1.2	2	2.5	1.3	2.5
r_i [cm]		4.76×10^{16}	1.91×10^{16}	1.73×10^{17}	8.18×10^{15}	1.88×10^{16}	2.46×10^{16}
r_o [cm]		3.48×10^{17}	1.53×10^{17}	6.88×10^{17}	2.05×10^{17}	1.88×10^{17}	3.11×10^{17}
$\dot{M}$ [$\frac{M_\odot}{yr}$]		3.48×10^{-5}	3.48×10^{-5}	1.09×10^{-3}	6.92×10^{-6}	8.93×10^{-5}	3.12×10^{-5}
v_{exp} [km s^{-*1}]		10 .0	15.5	35.0	12.0	16.0	10.0
M_d [$M_\odot$]		1.66×10^{-3}	4.35×10^{-4}	2.31×10^{-2}	1.63×10^{-4}	1.35×10^{-3}	1.28×10^{-3}
Ref.		1, 2, 3, 4	5, 6, 7, 18, 19, 20	3, 8, 9, 10, 18, 19, 21	11, 12, 13, 19, 22	14, 15, 18, 19, 20	13, 16, 17, 18

References - (1) Meixner et al. (2004); (2) Hony et al. (2003); (3) Hrivnak et al. (1989); (4)Van Genderen et al. (1986); (5) Ghedill et al. (2003); (6) Ueta et al. (2000); (7) Skinner et al. (1994); (8) Van der Veen (1994); (9) Hawkins et al. (1995); (10) Thévenin et al. (2000); (11) Kwok et al. (1995); (12) Hrivnak et al. (1995); (13) Volk et al. (2002); (14) Su et al. (2001); (15) Bujarrabal et al. (2001); (16) Hrivnak et al. (1991); (17) Ueta et al. (2001); (18) Walmsley et al. (1991); (19) Gledhill et al. (2002); (20) Likkel et al. (1991); (21) Bujarrabal et al. (1992); (22) Hrivnak et al. (2000).

(Hildebrand 1983). This value is a factor of 5 greater than the grain size obtained from the $n \propto a^{-6}$ distribution in the adopted range for a. Assuming $\chi_{850\ \mu m} = 0.54$ cm^2 g^{-1} (Gledhill & Yates 2003) for such a small grain radius, the derived dust mass increases by one order of magnitude.

The inner shell radius derived from the SED fit agrees with the value of 1400 AU (2.1×10^{16} cm at 1.2 kpc) obtained by Hoogzaad et al. (2002), but it is about 30–40% larger than the same parameter derived from Gledhill & Yates (2003) and Meixner et al. (2002), who nevertheless used an asymmetric dust model. The outer radius is larger than the values obtained from Hoogzaad et al. (2002) and Meixner et al. (2002), but close to the one derived by Gledhill & Yates (2003) and to the extension of 6.″5 derived from the CO observation (Bujarrabal et al. 1992).

IRAS 19114+0002 is an oxygen-rich object of spectral type G5 Ia (Hrivnak et al. 1989), but the real evolutionary status of this object is still controversial. It has been classified either as a post-AGB star having a luminosity of about 10^4 $L_\odot$ and lying at 1 kpc (Hrivnak et al. 1989) or as a massive red supergiant with luminosity near 3×10^5 $L_\odot$ and lying at a distance of 6 kpc (Hawkins et al. 1995).

The expansion velocity of the circumstellar envelope $v_e \approx 35$ km s^{-1} determined from the profile of the circumstellar CO emission (Zuckerman & Dyck 1986; Bujarrabal et al. 1992) is significantly higher than the typical value of 15 km s^{-1} for an AGB star, and it favours the supergiant hypothesis, which is still in doubt (Josselin & Lèbre 1992).

As for IRAS 17436+5003, Gledhill & Takami (2001) pointed out the need to adopt a steep power law for the grain size distribution, in order for it to agree with the high degrees of linear polarization observed in the near-IR. We thus adopted the grain size distribution $n \propto a^{-6}$ with $a_{\min} = 0.005$ μm and $a_{\max} = 0.25$ μm. The SED fit gives a $r_{\rm in} = 1.7 \times 10^{17}$ cm, which accords well with the inner shell radius of about 1.5×10^{17} cm obtained from both mid-IR images (Jura & Werner 1999) and near-IR imaging polarimetry observations (Gledhill et al. 2001). This value is very close to the inner shell size of 1.8×10^{17} cm as derived, when using the distance of 6 kpc, from high-resolution CO observations performed in Jura et al. (2001). The dust mass obtained is in good agreement with the one derived in Gledhill et al. (2002) on the basis of submillimeter observations.

IRAS 20000+3239. Low-resolution K-band spectra performed by Davis et al. (2003) showed a rather compact source with an angular size lower than 2″, and Hrivnak et al. (1999) measured a 1.″6 diameter in the V band. Compared with the SED parameters derived by Volk et al. (2002), we obtained good accordance in the derived values of both the mass-loss rate and inner shell radius, as well as for the shell mass derived from Gledhill et al. (2002).

IRAS 20028+3910. This object is characterised by a bipolar morphology, with the central object highly obscured in optical and near-IR (Su et al. 2001; Ueta et al. 2000). The SED, constructed with the data reported by Su et al. (2001 and references therein), thus shows a mid and far infrared peak much brighter than the one in the near-IR. Neri et al. (1998) fitted the CO 1–0 visibility data with an elliptical Gaussian component with a size of 3.5″ × 11.1″. The dust mass obtained from our 1.2 mm measures agrees very well with the value calculated from previous submillimeter data (Gledhill et al. 2002).

IRAS 22272+5435 is an extremely carbon rich object and, like IRAS 07134+1005, shows peculiar IR spectral features. From the analysis of CO 1–0 visibility data, Neri et al. (1998) measured an extended envelope size (*FWHM*) of 21″. From subarcsecond mid-IR imaging study (Ueta et al. 2001) the dust shell was found to have a toroidal structure with a 0.5″ inner radius, which corresponds to 1.1×10^{16} cm at 1.6 kpc. Our fit indicates an inner radius that is consistent with the one measured by Ueta et al. (2001) to within a factor of 2. A major discrepancy is found in the estimates of mass-loss rate. On the basis of their radiative transfer calculations, in fact, Ueta et al. (2001) derived a wind with $\dot{M} = 4.1 \times 10^{-6}$ $M_\odot$ yr^{-1}. Our value is closer to the mean mass-loss rate obtained from the CO study performed Bujarrabal et al. (2001), which is 1.8×10^{-5} $M_\odot$ yr^{-1}, when scaled for our assumed distance. The authors report a total nebular mass of 0.18 $M_\odot$, which gives a dust mass of 8.0×10^{-4} $M_\odot$ for an assumed gas-to-dust ratio of 220 and which agrees with our estimate.

5. Summary and outlook

We have presented the results of 1.2 mm continuum observations for a sample of 24 sources classified as post-AGB. Continuum emission was detected toward 11 objects, while uncertain detection is reported for two other sources.

The circumstellar dust masses were derived from our 1.2 mm measures, assuming that the emission is due to optically thin dust. For the sources where the distance is known, the circustellar dust masses range between about 6×10^{-4} $M_\odot$ and 2.4×10^{-3} $M_\odot$, with the exception of IRAS 19114+0002, whose post-AGB nature is, however, still in question. For the other objects, we derived lower dust masses, indicating a younger circumstellar envelope, but the errors in the choice of the common assumed distance could have affected the derived values.

For six of the detected sources, we compared the observed SEDs, constructed with additional data from the literature, and the model spectra obtained using a symmetric radiative transfer code. This allowed us to estimate some physical parameters of stars and envelopes that have been compared with previously results reported in the literature.

The high detection rate (≈46%) seems to support the goodness of our selection rules, and an extension of the millimetric survey to the remaining targets in our sample is necessary. Stars in our full sample belong to different evolutionary phases in the transition from AGB to PN, as the stars with optical counterpart should be more evolved. Once the full sample has been observed, the comparison between the derived physical properties of different envelopes will provide fundamental information on this evolutionary phase that has not yet been fully understood.

We still note that the CSEs surrounding this kind of objects appear to be good targets for the first light projects for future millimeter arrays such as the Atacama Large Millimeter Array (ALMA). From our fits we derived the typical dimensions of CSEs ranging from 1.5×10^{17} to 1.2×10^{18} cm, which, combined with the distances as reported in Table 3, correspond to angular sizes from a few arcsecs up to ≈13″. This implies that such CSEs can be, in principle, mapped in great detail with the foreseen ALMA angular resolutions by using a combination of both compact (to fully recover all the flux) and extended configurations (Wilson et al. 2005). The foreseen capabilities of ALMA will allow us to directly map the dusty envelopes at several millimetric and submillimetric frequencies, at least for the more compact sources of our sample and in general for post-AGB sources. This could provide a better constraints on the modeling of CSE. Furthermore, a detailed map of CSE could probe the possible presence structured morphologies that can be related to different mass-loss episodes suffered by the star during the AGB evolutionary phase.

To evaluate the possibility of actually resolving and mapping the CSEs of our sample, we need to compare the expected flux densities with the foreseen ALMA sensitivity at each frequency channel. From the fitted SEDs we then extrapolated the flux densities in the ALMA first light channels, namely 0.5, 0.6 0.9 1.3, 2, and 3 mm. Expected ALMA sensitivities were calculated by using the ALMA Sensitivity Calculator (`www.eso.org/projects/alma/science/bin/sensitivity.html`) in the case of first-light, assuming that only 8 antennae will be available, and in the case of the full (64 antennae) array. For both configurations, we derived a detection rate close to 100% over the 3σ at almost all frequencies. In Fig. 4 we show the expected percentage of the studied objects that ALMA allows to be observed with a dynamical range greater than 50. It is evident that ALMA will allow us not only to better sample the millimetric range of the source SEDs, that up to now is very poor, but also to obtain, in most cases, multifrequency high-resolution maps of the circumstellar matter surrounding the stars of our sample, extended to the sources belonging to the southern hemisphere.

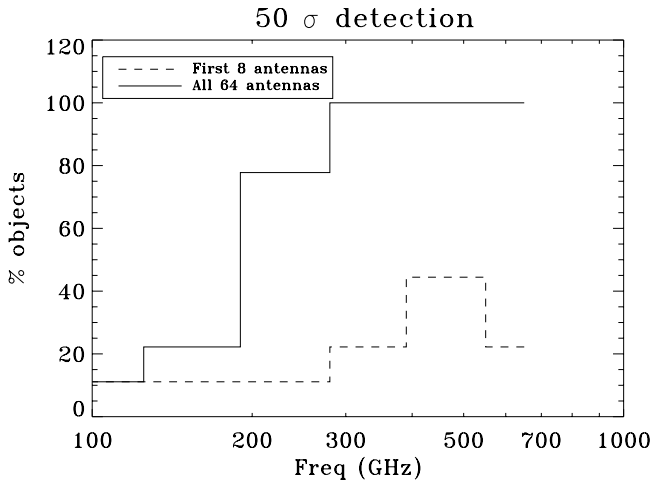

Fig. 4. Percentage of objects detected at 1.2 mm, that are observable with dynamical range greater than 50, assuming the ALMA sensitivity calculated with both 8 and 64 antennae.

Acknowledgements. We would like to thank the anonymous referee for the constructive criticism that enabled us to improve this paper.

References

Balick, B., & Frank, A. 2002, ARA&A, 40,439
Bujarrabal, V., Alcolea, J., & Planesas, P. 1992, A&A, 257, 701
Bujarrabal, V., Castro-Carrizo, A., Alcolea, J., & Sánchez Contreras, C. 2001, A&A, 377, 868
Clark, J. S., Egan, M. P., Crowther, P. A., et al. 2003, A&A, 412, 185
Davis, C. J., Smith, M. D., Stern, L., Kerr, T. H., & Chiar, J. E. 2003, MNRAS, 344, 262
Frank, A., Balick, B., & Livio, M. 1997, Planetary nebulae, ed. H. J. Habing, & H. J. G. L. M. Lamers, IAU Symp., 180, 225
Garcia-Lario, P., Manchado, A., Pych, W., & Pottash, S. R. 1997, A&AS, 126, 479
García-Segura, G., López, J. A., & Franco, J. 2005, ApJ, 618, 919
Gledhill, T. M., & Takami, M. 2001, MNRAS, 328, 266
Gledhill, T. M., & Yates, J. A. 2003, MNRAS, 343, 880
Gledhill, T. M., Bains, I., & Yates, J. A. 2002, MNRAS, 332, L55
Hawkins, G. W., Skinner, C. J., Meixner, M. M., et al. 1995, 452, 314
Hildebrand, R. H. 1983, QJRAS, 24, 267
Hrivnak, B. J. 1995, ApJ, 438, 341
Hrivnak, B. J., & Bieging, J. H. 2005, ApJ, 624, 331
Hrivnak, B. J., & Kwok, S. 1991, ApJ, 371, 631
Hrivnak, B. J., Kwok, S., & Volk, K. M. 1989, ApJ, 346, 265
Hrivnak, B. J., Langill, P. P., Su, K. Y. L., & Kwok, S. 1999, ApJ, 513, 421
Hrivnak, B. J., Volk, K., & Kwok, S. 2000, ApJ, 535, 275
Hony, S., Tielens, A. G. G. M., Waters, L. B. F. M., & de Koter, A. 2003, A&A, 402, 211
Hoogzaad, S. N., Molster, F. J., Dominik, C., et al. 2002, A&A, 389, 547
Huggins, P. J., Muthu, C., Bachiller, R., Forveille, T., & Cox, P. 2004, A&A, 414, 581
Ivezić, Z., Nenkova, M., & Elitzur, M. 1999, User Manual for DUSTY, University of Kentucky Internal Report
Josselin, E., & Lèbre, A. 2001, A&A, 367, 826
Jura, M., & Werner, M. W. 1999, ApJ, 525, L113
Jura, M., Chen, C., & Werner, M. 2000, ApJ, 544, L141
Jura, M., Velusamy, T., & Werner, M. W. 2001, ApJ, 556, 408
Justtanont, K., Barlow, M. J., Skinner, C. J., & Tielens, A. G. G. M. 1992, ApJ, 392, L75
Kelly, D. M., & Hrivnak, B. J. 2005, ApJ, 629, 1040
Kreysa, E., Gemuend, H.-P., Gromke, J., et al. 1998, SPIE, 3357, 319
Kwok, S., Volk, K. M., & Hrivnak, B. J. 1989, ApJ, 345, L51
Kwok, S., Hrivnak, B. J., & Geballe, T. R. 1995, ApJ, 454, 394
Likkel, L., Forveille, T., Omont, A., & Morris, M. 1991, A&A, 246, 153
Mathis, J. S., Rumpl, W., & Nordsieck, K. H. 1977, ApJ, 217, 425
Meixner, M., Ueta, T., Bobrowsky, M., & Speck, A. 2002, ApJ, 571, 936
Meixner, M., Zalucha, A., Ueta, T., Fong, D., & Justtanont, K. 2004, ApJ, 614, 371
Neri, R., Kahane, C., Lucas, R., Bujarrabal, V., & Loup, C. 1998, A&AS, 130, 1
Oudmaijer, R. D. 1996, A&A, 306, 823
Oudmaijer, R. D., van der Veen, W. E. C. J., Waters, L. B. F. M., et al. 1992, A&A, 96, 625
Pasquali, A., & Comerón, F. 2002, A&A, 389, 874
Pollack, J. B., Hollenbach, D., Beckwith, S., et al. 1994, ApJ, 421, 615
Pottasch, S. R., & Parthasarathy, M. 1988, A&A, 192, 182
Sahai, R., & Trauger, J. T. 1998, AJ, 116, 1357
Sahai, R. 2000, Post-AGB Objects as a Phase of Stellar Evolution, ed. R. Szczerba, & S. K. Grny, Ap.S.S.L., 265, 53
Skinner, C. J., Meixner, M. M., Hawkins, G. W., et al. 1994, ApJ, 423, L135
Su, K. Y. L., Hrivnak, B. J., & Kwok, S. 2001, AJ, 122, 1525
Thévenin, F., Parthasarathy, M., & Jasniewicz, G. 2000, A&A, 359, 138
Trams, N. R., Waters, L. B. F. M., Waelkens, C., et al. 1991, A&A SS 87, 361
Ueta, T., Meixner, M., & Bobrowsky, M. 2000, ApJ, 528, 861
Ueta, T., Meixner, M., Hinz, P. M., et al. 2001, ApJ, 557, 831
Umana, G., Buemi, C. S., Trigilio, C., & Leto, P. 2005, A&A, 437, L1
van der Veen, W. E. C. J., Waters, L. B. F. M., Trams, N. R., & Matthews, H. E. 1994, A&A, 285, 551
van Genderen, A. M., Greidanus, H., & van Driel, W. 1986, A&A, 155, 72
van Winckel 1997, A&A, 319, 561
van Winckel, H., & Reyniers, M. 2000, A&A, 354, 135
Volk, K., Kwok, S., Hrivnak, B. J., & Szczerba, R. 2002, ApJ, 567, 412
ilson, T. L., Beasley, A. J., & Wootten, H. A. 2005, in The Cool Universe: Observing Cosmic Dawn, ASP Conf. Ser., 344, 232
Walmsley, C. M., Chini, R., Kreysa, E., et al. 1991, A&A, 248, 555
Zuckerman, B., & Dyck, H. M. 1986, ApJ, 311, 345
Zylka, R. 1998, Pocket Cookbook for MOSPI Software, `http://iram.fr/IRAMES/otherDocuments/manuals/Datared/pockcoo.ps`